Geometries, Electronic Structures and Vibrational Spectral Studies of 4-Aminopyridine-2-Carbonitrile (4AP2CN) Dye Using Quantum Chemical Calculations for Dye Sensitized Solar Cells

P.SAKTHIVEL[a], K.PERIYASAMY[b],I.RAGAVAN[c] P.M.ANBARASAN[c]

a. Department of Physics, Selvamm Arts & Science college, Namakkal – 637 003,Tamilnadu, India

b. Department of Physics, Vaigai Arts & Science women's college,Valapady – 636 111,Salem, Tamilnadu, India.

c. Department of Physics, Periyar University,Salem – 636011, Tamilnadu, India.

Abstract

Quantum chemical calculations can provide information about geometrical and electronic structure at a detailed level. The calculation of polarizability and hyperpolarizability reveals the NLO of the system. In this chapter a nitrile dye sensitizer 4AP2CN (CAS Number: 98139-15-2) is selected for our study. Its linear formula is $C_6H_5N_3$ and molecular weight is 119.12400 [g/mol]. The performance of this metal free 4AP2CN dye that can be used in DSSC is studied and results are discussed.

7.1 Introduction

The new technologies for direct solar energy conversion have gained more attention in the last few years. In particular, Dye Sensitized Solar Cells (DSSCs) are promising in terms of efficiency and low cost [1-3]. The foremost feature of DSSC consists in a wide band gap nanocrystalline film grafted with a quasi-monolayer of dye molecules and submerged in a redox electrolyte. This elegant architecture can synchronously address two critical issues of employing organic materials for the photovoltaic applications: (i) efficient charge generation from the Frenkel excitons; (ii) long-lived electron-hole separation up to the millisecond time domain. The latter attribute can often confer an almost quantitative charge collection for several micrometer-thick active layers, even if the electron mobilities in nanostructured semiconducting films are significantly lower than those in the bulk crystalline materials. Benefited from systematic device engineering and continuous material innovation, a state of the art DSSC with a ruthenium sensitizer has achieved a validated efficiency of 11.1% [4] measured under the air mass 1.5 global (AM1.5G) conditions. In view of the limited ruthenium resource and the heavy-metal toxicity, metal-free organic dyes have received surging research interest in recent years. Because of their high molar absorption coefficient, relatively simple synthesis procedure, various structures and lower cost in contrast to a ruthenium dye and the flexibility in molecular tailoring of an organic sensitizer provides a large area to explore [5-7]. Meanwhile, recently a

rapid progress of organic dyes has been witnessed reaching close to 10.0% efficiencies in combination with a volatile acetonitrile-based electrolyte [8]. In this Chapter the performance of 4AP2CN metal free dye that can be used in DSSC is analyzed.

2. Experimental Techniques

The compound 4AP2CN Dye was obtained from Sigma-Aldrich Chemical Company, USA with a stated purity of greater than 99% and it was used as such without further purification. The FT-Raman spectrum of 4AP2CN Dye has been recorded using 1064 nm line of Nd: YAG laser as excitation wavelength in the region 50-3500 cm^{-1} on a Brucker model IFS 66 V spectrophotometer. The FT-IR spectrum of this compound was recorded in the region 400-4000 cm^{-1} on IFS 66 V spectrophotometer using KBr pellet technique. The spectrum was recorded at room temperature, with scanning speed of 30 $cm^{-1}min^{-1}$ and the spectral resolution of 2.0 cm^{-1}.

3. Theoretical background of 4AP2CN

Density functional theory (DFT) and Time dependant- Density Functional Theory (TD-DFT) calculations were performed to determine geometries, electronic structures and electronic Absorption spectra of the selected Dye. All the calculations, both in gas and solvent phase, were performed using Gaussian09w package [9]. The DFT was treated according to Becke's three parameter gradient-corrected exchange potential and the Lee-Yang-Parr gradient-corrected correlation potential (B3LYP) [10–11], and all calculations were performed without any symmetry constraints by using polarized split-valence 6-311++G (d, p) basis sets. The electronic absorption spectrum requires calculation of the allowed excitations and oscillator strengths. These calculations were done using TD-DFT with the same basis sets and exchange-correlation functional in vacuum and solution, and the non-equilibrium version of the polarizable continuum model (PCM) [12, 13] was adopted for calculating the solvent effects.

4. Results and Discussion

4.1. The Geometric Structure

The optimized geometry of the 4AP2CN Dye is shown in **Fig. 1.** The bond lengths, bond angles and dihedral angles are listed in **Table 1.** Since the crystal structure of the exact title compound is not available till now, the optimized structure can be only be compared with other similar systems for which the crystal structures have been solved. From the theoretical values we can find that most of the optimized bond lengths, bond angles and dihedral angles. The distance between C1 and N6 atoms in cyanine groups of 4AP2CN Dye are 1.3193 Å and 1.3417 Å respectively at B3LYP/6-311++G (d,p) and also compared with HF/6-311++G (d,p).

4.2. Electronic Structures and Charges

Natural Bond Orbital (NBO) analysis was performed in order to analyze the charge populations of the dye 4AP2CN. Charge distributions in C, N and H atoms were observed because of the different electro-negativity, the electrons transferred from C atoms to C, N atoms, C atoms to H and N atoms to H atom. The natural charges of different groups are the sum of every atomic natural charge in the group. These data indicate that the cyanine groups are donors and amide groups is acceptor and the charges were transferred through chemical bonds. The frontier molecular orbitals (MO) energies and corresponding density of state of the dye 4AP2CN Dye is shown in **Fig. 2.** The HOMO–LUMO gap of the dye 4AP2CN Dye in vacuum is 5.17 eV.

While the calculated HOMO and LUMO energies of the bare $Ti_{38}O_{76}$ cluster as a model for nanocrystalline are -6.55 and -2.77eV, respectively, resulting in a HOMO–LUMO gap of 3.78 eV, the lowest transition is reduced to 3.20 eV according to TDDFT, and this value is slightly smaller than typical band gap of TiO_2 nanoparticles with nm size [14]. Furthermore, the HOMO, LUMO and HOMO–LUMO gap of $(TiO_2)_{60}$ cluster is -7.52, -2.97, and 4.55 eV (B3LYP/VDZ), respectively [15]. Taking into account of the cluster size effects and the calculated HOMO, LUMO, HOMO–LUMO gap of the dye 4AP2CN Dye, $Ti_{38}O_{76}$ and $(TiO_2)_{60}$ clusters, we can find that the HOMO energies of these dyes fall within the TiO_2 gap.

The above data also reveal the interfacial electron transfer between semiconductor TiO_2 electrode and the dye sensitizer 4AP2CN Dye is electron injection processes from excited dye to the semiconductor conduction band. This is a kind of typical interfacial electron transfer reaction [16].

4.3. IR and Raman Frequencies

Fig. 4 and **5** shows the observed and calculated IR and Raman spectra of 4AP2CN Dye respectively. Comparison of the observed (FT-IR and FT-Raman) and calculated vibrational frequencies of 4AP2CN Dye is shown in **Table 2.** Comparison of the frequencies calculated by ab initio HF and B3LYP with experimental values reveals the overestimation of the calculated vibrational modes due to neglect of anharmonicity in real system. Inclusion of electron correlation in density functional theory to a certain extent makes the frequency values smaller in comparison with experimental values. Any way notwithstanding the level of calculations it is customary to scale down the calculated harmonic frequencies in order to improve the agreement with the experiment. In our study we have followed two different scaling factors B3LYP/6-311++G (d,p) and HF/6-311++G(d,p). The 4AP2CN Dye molecule give rise to three C-H stretching, one C-H wagging vibrations, four C-H in-plane bending vibration, one C-C-N stretching vibration, one C-C-N torsion vibration, four C=C stretching vibrations, one C-N stretching vibrations, three ring deformation vibrations and one ring torsion vibrations were assigned, six C-C-N Wagging Vibrations, Three C-C-N inplane Bending one C-N out of plane Bending, one C-H out of plane Bending, one C-NH2 wagging, four overtone combination, one

NH2 symmetric Stretching, three NH2 Asymmetric Stretching. The strongest IR absorption for 4AP2CN corresponds to the vibrational mode 29 near about 1720 cm^{-1}, which is the stretching mode of C-C bonds. The next stronger IR absorption is attributed to vibrational mode 32 near about 3340 cm^{-1}, corresponding to stretching mode of C=H bonds. In the Raman spectra, however, the strongest activity mode is the vibrational mode 31 near about 2950 cm^{-1}, which is corresponding to stretching mode of C-H bond.

4.4. Polarizability and Hyperpolarizability

Polarizabilities and hyperpolarizabilities characterize the response of a system in an applied electric field [17]. They determine not only the strength of molecular interactions (long-range intermolecular induction, dispersion forces, etc.) as well as the cross sections of different scattering and collision processes, but also the nonlinear optical properties (NLO) of the system [18, 19]. It has been found that the dye sensitizer hemicyanine system, which has high NLO property, usually possesses high photoelectric conversion performance [20]. In order to investigate the relationships among photocurrent generation, molecular structures and NLO, the polarizabilities and hyperpolarizabilities of 4AP2CN Dye was calculated.

The polarizabilities and hyperpolarizabilities could be computed via finite field (FF) method, sum-over state (SOS) method based on TD-DFT, and coupled-perturbed HF (CPHF) method. However, the use of FF, SOS, and CPHF methods with large sized basis sets for 4AP2CN is too expensive. Here, the polarizability and the first hyperpolarizabilities are computed as a numerical derivative of the dipole moment using B3LYP/6-311++G (d,p).

Tables 3 and **4** list the values of the polarizabilities and hyperpolarizabilities of the dye 4AP2CN Dye. In addition to the individual tensor components of the polarizabilties and the first hyperpolarizabilities, the isotropic polarizability, polarizability anisotropy invariant and hyperpolarizability are also calculated. The calculated isotropic polarizability of 4AP2CN Dye is 9.6507 a.u. However, the calculated isotropic polarizability of JK16, JK17, dye 1, dye 2, D5, DST and DSS is 759.9, 1015.5, 694.7, 785.7, 510.6, 611.2 and 802.9 a.u., respectively [21,22]. The above data indicate that the donor-conjugate p bridge-acceptor (D-π-A) chain-like dyes have stronger response for external electric field. Whereas, for dye sensitizers D5, DST, DSS, JK16, JK17, dye 1 and dye 2, on the basis of the published photo-to-current conversion efficiencies, the similarity and the difference of geometries, and the calculated isotropic polarizabilities, it is found that the longer the length of the conjugate bridge in similar dyes, the larger the polarizability of the dye molecule, and the lower the photo-to-current conversion efficiency. This may be due to the fact that the longer conjugate-π-bridge enlarged the delocalization of electrons, thus it enhanced the response of the external field, but the enlarged delocalization may be not favorable to generate charge separated state effectively. So it induces the lower photo-to-current conversion efficiency.

4.5. Electronic Absorption Spectra and Sensitized Mechanism

In order to understand the electronic transitions of 4AP2CN Dye, TD-DFT calculations on electronic absorption spectra in vacuum and solvent were performed, and the results are shown in **Fig. 6**. It is observed that, for 4AP2CN Dye, the absorption in the visible region is much weaker than that in the UV region. The calculated results have a red-shift. The results of TD-DFT have an appreciable red-shift, and the degree of red-shift in solvent is more significant than that in vacuum. The discrepancy between vacuum and solvent effects in TD-DFT calculations may result from two aspects. The first aspect is smaller gap of materials which induces smaller excited energies. The other is solvent effects. Experimental measurements of electronic absorptions are usually performed in solution. Solvent, especially polar solvent, could affect the geometry and electronic structure as well as the properties of molecules through the long-range interaction between solute molecule and solvent molecule. For these reasons it is more difficult to make the TD-DFT calculation is consistent with quantitatively. Though the discrepancy exists, the TD-DFT calculations are capable of describing the spectral features of 4AP2CN Dye because of the agreement of line shape and relative strength as compared with the vacuum and solvent. The HOMO-LUMO gap of 4AP2CN Dye in acetonitrile at B3LYP/6-311++G (d, p) theory level is smaller than that in vacuum. This fact indicates that the solvent effects stabilize the frontier orbitals of 4AP2CN Dye. So it induces the smaller intensities and red-shift of the absorption as compared with that in vacuum. In order to obtain the microscopic information about the electronic transitions, the corresponding MO properties are checked. The absorption in visible and near-UV region is the most important region for photo-to-current conversion, so only the 20 lowest singlet/singlet transitions of the absorption band in visible and near-UV region for 4AP2CN is listed in Table 7.5. The data of Fig.7.6 are based on the 6-311++G (d, p) results with solvent effects involved. Where I_0 is the photon flux, *Jsc* is the short-circuit photocurrent density, and *Voc* is the open-circuit photo voltage, and ff represents the fill factor [23]. At present, the J_{sc}, the V_{oc}, and the *ff* are only obtained by experiment, the relationship among these quantities and the electronic structure of dye is still unknown.

The analytical relationship between V_{oc} and E_{LUMO} may exist. According to the sensitized mechanism the transitions are photo induced charge transfer processes, thus the excitations generate charge separated states, which should favour the electron injection from the excited dye to semiconductor surface.

The solar energy to electricity conversion efficiency (η) under AM 1.5 white-light irradiation can be obtained from the following formula: refer eq. (2.4). On the excited dyes to the semiconductor conduction band) and single electron and single state approximation, there is an energy relationship: refer eq. (2.5).Where, E_{CB} is the energy of the semiconductor's conduction band edge. So the Voc may be obtained applying the following formula: refer eq. (2.5)

It induces that the higher the E_{LUMO}, the larger the V_{oc}. The results of organic dye sensitizer JK16 and JK17 [21], D-ST and D-SS also proved the tendency [24] (JK16: LUMO = -2.73 eV, V_{oc} = 0.74 V; JK17: LUMO = -2.87 eV, V_{oc} = 0.67 V; D-SS: LUMO = -2.91 eV, V_{oc} = 0.70 V; D-ST: LUMO = -2.83 eV, V_{oc} = 0.73 V). Certainly, this formula expects further test by experiment and theoretical calculation**.** The J_{sc} is determined by two processes, one is the rate of electron injection from the excited dyes to the conduction band of semiconductor, and the other is the rate of redox between the excited dyes and electrolyte. Electrolyte effect on the redox processes is very complex, and it is not taken into account in the present calculations. This indicates that most of excited states of 4AP2CN Dye have larger absorption coefficient, and then with shorter lifetime for the excited states, so it results in the higher electron injection rate which leads to the larger Jsc of 4AP2CN Dye. On the basis of above analysis, it is clear that the 4AP2CN Dye has better performance in DSSC.

5. Conclusion

The geometries, electronic structures, polarizabilities, and hyperpolarizabilities of dye 4AP2CN was studied by using ab initio HF and density functional theory with hybrid functional B3LYP, and the UV-Vis spectra were investigated by using TD-DFT methods. The NBO results suggest that 4AP2CN Dye is a (D-π-A) system. The calculated isotropic polarizability of 4AP2CN Dye is 59.57 a.u. The calculated polarizability anisotropy invariant of 4AP2CN Dye is 9.65 a.u. The hyperpolarizability of 4AP2CN Dye is 11.96 (in a.u). The 4AP2CN Dye molecule give rise to three C-H stretching, one C-H wagging vibrations, four C-H in-plane bending vibration, one C-C-N stretching vibration, one C-C-N torsion vibration, four C=C stretching vibrations, one C-N stretching vibrations, three ring deformation vibrations and one ring torsion vibrations were assigned, six C-C-N Wagging Vibrations, Three C-C-N inplane Bending one C-N out of plane Bending, one C-H out of plane Bending, one C-NH_2 wagging, four overtone combination, one NH_2 symmetric Stretching, three NH_2 Asymmetric Stretching. The strongest IR absorption for 4AP2CN Dye corresponds to the vibrational mode 29 near about 1720 cm^{-1}, which is the stretching mode of C-C bonds. The next stronger IR absorption is attributed to vibrational mode 32 near about 3340 cm^{-1}, corresponding to stretching mode of C=H bonds. In the Raman spectra, however, the strongest activity mode is the vibrational mode 31 near about 2950 cm^{-1}, which is corresponding to stretching mode of C-H bond.

The electronic absorption spectral features in visible and near-UV region were assigned based on the qualitative agreement to TD-DFT calculations. The absorptions are all ascribed to π→π* transition. The three excited states with the lowest excited energies of 4AP2CN Dye is photoinduced electron transfer processes that contributes sensitization of photo-to-current conversion processes. The interfacial electron transfer between semiconductor TiO_2 electrode and dye sensitizer 4AP2CN Dye is electron injection process from excited dye as donor to the semiconductor conduction band. Based on the analysis of geometries, electronic structures, and

spectrum properties between 4AP2CN Dye the role of cyanine and amine group is as follows: it enlarged the distance between electron donor group and semiconductor surface, and decreased the timescale of the electron injection rate, resulted in giving lower conversion efficiency. This indicates that the choice of the appropriate conjugate bridge in dye sensitizer is very important to improve the performance of DSSC.

Fig. 1 Optimized geometrical structure of dye 4AP2CN

Fig. 2 Isodensity plots (isodensity contour = 0.02 a.u.) of the frontier orbitals of

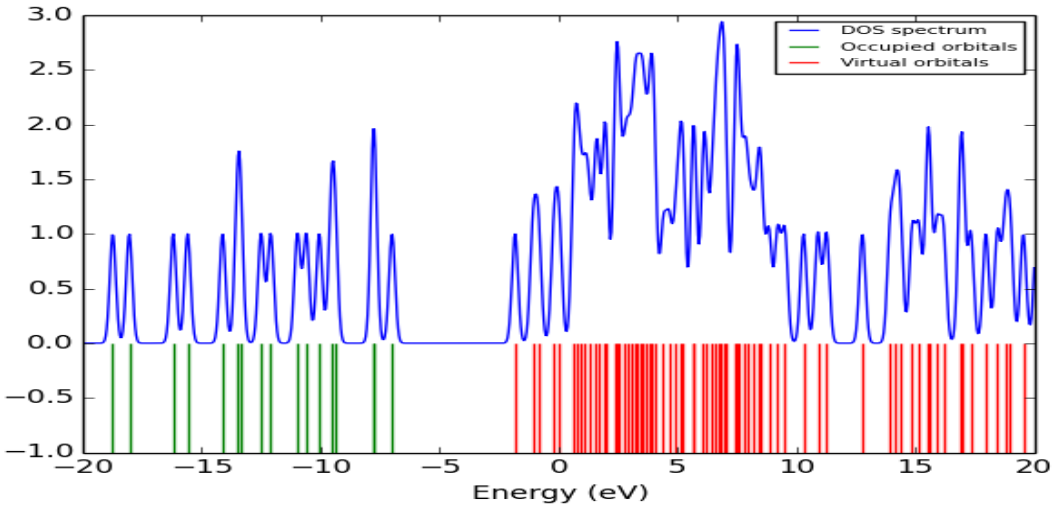

Fig.3. The frontier molecular orbital energies and corresponding DOS spectrum of the dye 4AP2CN

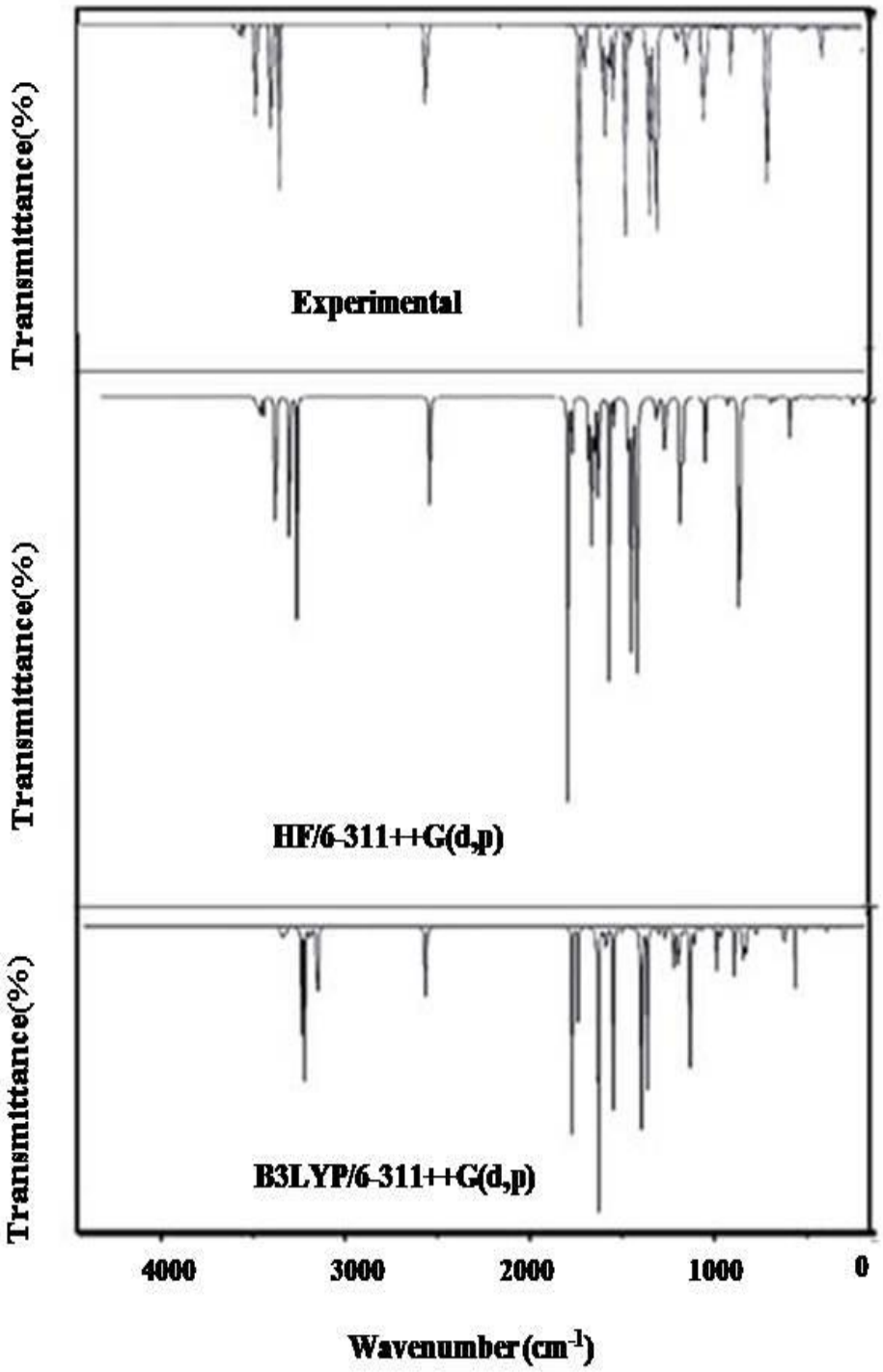

Fig. 4 Observed and Calculated FT-IR Spectra of 4AP2CN

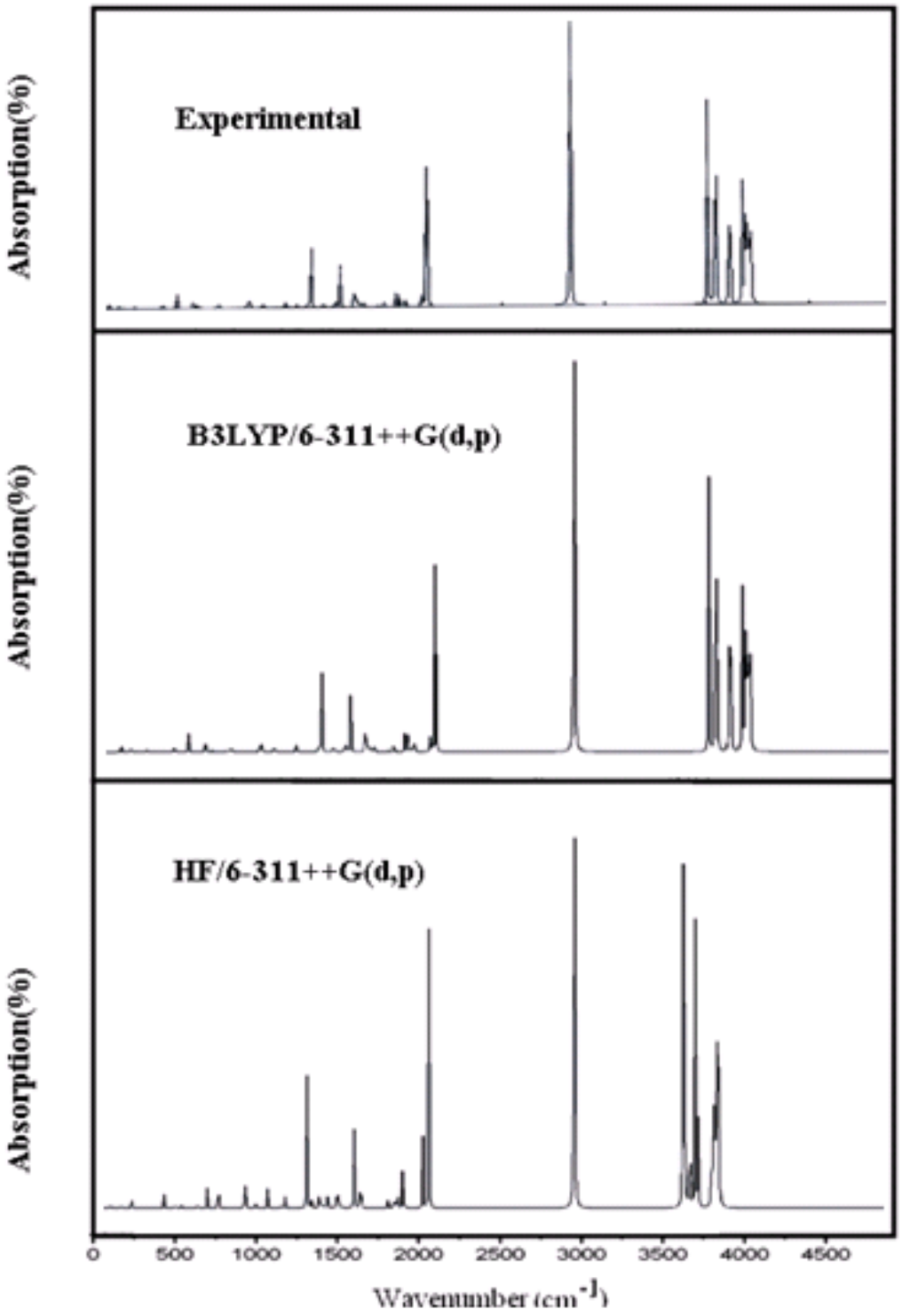

Fig. 5 Observed and Calculated FT-Raman Spectra of 4AP2CN.

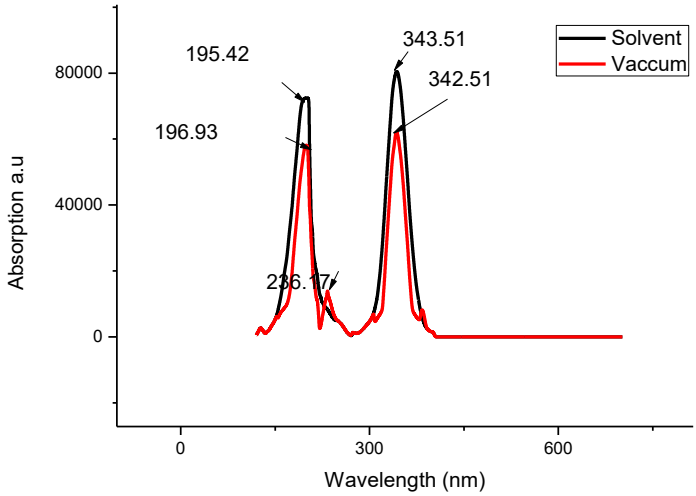

Fig. 6 calculated electronic absorption spectra of the dye 4AP2CN.

Table 1 Bond lengths (in Angstrom), bond angles (in degree) and dihedral angles (in degree) of the dye 4AP2CN

Parameters	**HF/6-311++G(d,p)**	**DFT/B3LYP/6-311++G(d,p)**
Bond length (Å)		
C1-C2	1.3787	1.3925
C1-N6	1.3193	1.3417
C1-C7	1.4548	1.4434
C2-C3	1.3956	1.4051
C2-H10	1.0739	1.0837
C3-C4	1.3926	1.4054
C3-N9	1.3716	1.3669
C4-C5	1.3803	1.3879
C4-H11	1.0749	1.0845
C5-C6	1.3193	1.3357
C5-H12	1.0761	1.0862
C7-N8	1.1296	1.1544
N9-H13	0.9939	1.0052
N9-H14	0.9939	1.005
Bond Angle (°)		
C2-C1-N6	125.2364	124.8627
C2-C1-C7	118.3876	118.5373
N6-C1-C7	116.3758	116.5999
C1-C2-C3	118.179	118.6716
C1-C2-H10	120.4041	120.1632
C3-C2-H10	121.4164	121.1652
C2-C3-C4	117.0887	116.8545
C2-C3-N9	121.1347	121.3321
C4-C3-N9	121.7386	121.8128
C3-C4-C5	118.9402	119.2232
C3-C4-H11	120.9249	120.6984
C5-C4-H11	120.1344	120.0783
C4-C5-C6	124.4307	124.6662
C4-C5-H12	119.6141	119.6001

Continue

C6-C5-H12	115.9553	115.7336
C1-N6-H12	116.1247	115.7216
C3-N9-H13	117.3658	121.107
C3-N9-H14	117.2541	121.0014
H13-N9-H14	114.0746	117.7447
Dihedral Angle (°)		
C1-C7-N8-C2-C-1	178.1198	178.0004
C1-C7-N8-C2-C-2	179.9605	179.9911
N6-C1-C2-C3	0.0574	0.0296
N6-C1-C2-H10	-179.6972	-179.9505
C7-C1-C2-C3	-179.8175	-179.9969
C7-C1-C2-H10	0.4279	0.0296
C2-C1-N6-C5	0.0876	-0.0132
C7-C1-N6-C5	179.9647	-179.9937
C1-C2-C3-C4	-0.1895	-0.0056
C1-C2-C3-N9	-177.9875	-179.7506
H10-C2-C3-C4	179.5624	179.9677
H10-C2-C3-N9	1.7662	0.2227
C2-C3-C4-C5	0.1821	-0.0189
C2-C3-C4-H11	-179.5598	-179.9732
N9-C3-C4-C5	177.9641	179.7248
N9-C3-C4-H11	-1.7779	-0.2295
C2-C3-N9-H13	-20.3653	-2.3219
C2-C3-N9-H14	-161.9303	-177.817
C4-C3-N9-H13	161.9418	177.9458
C4-C3-N9-H14	20.3767	2.4507
C3-C4-C5-N6	-0.0391	0.0306
C3-C4-C5-H12	179.9378	179.9975
H11-C4-C5-N6	179.7049	179.9852
H11-C4-C5-H12	-0.3182	-0.0479
C4-C5-N6-C1	-0.0969	-0.0142
H12-C5-N6-C1	179.9254	-179.9823

Table 2 Comparison of the observed (FT-IR and FT-Raman) and calculated vibrational frequencies of 4AP2CN.

Vibrational mode no.	Species	Experimental		Scaled Wavenumber (cm^{-1})		IR Intensity	Raman active	Depolarisation Ratio	Reduced Mass	Force Constants	Assignments
		FT-IR	FT-Raman	HF/6-311G(d,p)	B3LYP/6-311G(d,p)						
1	A''	-	-	152.6091	-246.5308	224.0397	0.9803	0.2098	1.2454	0.0446	C-C-N wagging
2	A'	-	-	171.9647	137.2793	0.6311	0.2315	0.7488	5.7492	0.0638	C-C-N in plane bending
3	A'	-	-	238.6923	155.4667	2.6924	4.7140	0.7403	7.9106	0.1127	C-C-N wagging
4	A'	-	-	369.5364	214.9821	0.1035	0.1527	0.7409	4.8090	0.1310	C-C-N wagging
5	A'	-	-	406.2720	375.2775	1.5634	1.4423	0.7283	3.0714	0.2549	C-C-N wagging
6	A'	-	-	425.0493	380.0399	0.6703	1.3563	0.7500	4.5598	0.3880	C-C-N wagging
7	A''	485	470	482.7021	420.6864	0.2089	0.1143	0.7500	1.0245	0.1068	C N out-of-plane bending/C-C-N wagging
8	A''	500	-	513.4133	481.6300	0.7703	3.3680	0.2649	9.3717	1.2808	Ring torsion
9	A'	-	-	548.6377	497.2011	24.4533	1.1812	0.7202	3.4607	0.5041	Ring deformation
10	A'	-	-	574.9701	538.0358	0.9151	8.5591	0.2853	7.1284	1.2158	Ring deformation
11	A'	685	-	646.9890	592.0641	3.4358	1.5883	0.7170	7.3816	1.5245	Ring deformation
12	A'	-	-	726.0421	658.5635	2.9770	1.6178	0.6997	4.7239	1.2071	C-NH2 Wagging
13	A''	820	-	818.0837	749.4983	0.7865	0.8794	0.7437	3.1979	1.0584	C-H stretching
14	A'	-	-	823.9859	766.6679	2.7063	14.5322	0.1146	6.9968	2.4231	C-C-N in plane bending
15	A'	-	-	926.5744	840.2415	23.8482	0.2405	0.6083	1.4767	0.6143	C-C-N in plane bending
16	A''	-	972	965.4197	874.3600	18.0960	0.1165	0.4953	1.6219	0.7305	C-C-N torsion
17	A''	1010	-	1021.6497	959.2339	15.7643	10.1978	0.0811	3.3148	1.7970	Overtone/combination

Continue

18	A’	-	-	1082.1882	985.8642	0.2764	0.2337	0.7470	1.3737	0.7866	Overtone/combination
19	A’’	1100	-	1106.7269	999.9074	27.7004	35.4394	0.0703	7.5174	4.4283	Overtone/combination
20	A’’	-	-	1149.0784	1054.2092	3.4067	0.3778	0.2056	1.5245	0.9982	Overtone/combination
21	A’	1250	-	1203.8256	1128.6232	7.4541	5.4690	0.2812	1.5054	1.1298	C-N stretching
22	A’’	1270	1210	1274.2482	1187.0006	13.5722	18.1400	0.1991	1.7909	1.4867	NH2 twisting C-H wagging
23	A’	-	-	1296.0809	1309.3468	15.9794	2.3530	0.7495	5.7747	5.8330	C-H in plane bending
24	A’	1440	-	1418.8703	1316.4590	23.4776	6.5684	0.2132	1.7056	1.7416	C-H in plane bending
25	A’	-	1500	1450.9363	1365.3901	38.4473	20.6655	0.1694	2.5349	2.7843	C-H in plane bending
26	A’	1500	1540	1578.7439	1458.1442	9.2421	20.3083	0.4410	3.4302	4.2971	C-H out of plane bending
27	A’	1520	-	1646.1276	1507.4824	31.9186	2.8330	0.7169	2.6913	3.6034	C H in-plane bending C=C stretching
28	A’	-	1800	1758.9986	1594.3332	46.2760	35.4844	0.4035	6.5424	9.7982	C NH2 stretching C=C stretching
29	A’	1720	2020	1776.0481	1631.0744	141.9637	28.8093	0.4373	3.1101	4.8749	C=C stretching
30	A’	2010	2480	1810.9425	1659.7386	330.2439	13.7611	0.6993	1.4416	2.3398	C=C stretching + C-C-N stretching
31	A’	2540	2920	2594.3778	2341.5774	10.1661	418.5334	0.2756	12.6871	40.9853	C=H stretching
32	A’	3340	-	3327.9001	3154.8448	12.2987	91.4283	0.5052	1.0885	6.3830	C=H stretching
33	A’	3415	3750	3347.6072	3177.6309	14.5019	164.0280	0.2048	1.0944	6.5106	N-H2 symmetric stretching
34	A’	3430	3800	3353.6018	3183.4188	2.7690	90.2601	0.2605	1.0923	6.5218	N-H2 Asymmetric stretching
35	A’	3490	3920	3810.5450	3621.4557	86.8035	190.2026	0.1407	1.0454	8.0778	N-H2 Asymmetric stretching
36	A’	3520	4000	3919.9637	3739.9493	44.1108	51.7882	0.7447	1.1052	9.1083	N-H2 Asymmetric stretching

Table 3 Polarizability (α) of the dye 4AP2CN (in a.u.).

α_{xx}	α_{xy}	α_{yy}	α_{xz}	α_{yz}	α_{zz}	α	Δα
-58.282	-3.7468	-46.5939	0.3394	-0.1835	-54.9214	59.5793	9.6507

Table 4 Hyperpolarizability (β) of the dye 4AP2CN (in a.u.).

β_{xxx}	β_{xxy}	β_{xyy}	β_{yyy}	β_{xxz}	β_{xyz}	β_{yyz}	β_{xzz}	β_{yzz}	β_{zzz}	β_{ii}
113.6247	3.4038	25.5794	-13.6089	1.9564	-0.5208	0.8599	-1.9846	-0.1306	0.5908	11.9623

Table 5 Computed excitation energies, electronic transition configurations and oscillator strengths (f) for the optical transitions with f > 0.01 of the absorption bands in visible and near- UV region for the 4AP2CN dye in acetonitrile.

State	Configurations composition (corresponding transition orbitals)	Excitation energy (eV/nm)	oscillator strength (f)
1	HOMO->LUMO (95%)	4.5598/346	0.8248
2	H-1->LUMO (75%)	4.5665/342	0.0040
3	HOMO->L+1 (80%)	5.3057/336	0.0028
4	H-2->LUMO (90%)	5.3295/331	0.0060
5	H-1->L+1 (68%)	5.4481/327	0.0566
6	H-8->LUMO (79%)	6.0287/322	0.0015
7	H-3->LUMO (10%), H-1->L+2 (11%), HOMO->L+2 (60%)	6.0325/315	0.4656
8	H-4->LUMO (11%), H-3->LUMO (68%), H-1->L+1 (10%)	6.1936/308	0.0039
9	H-4->LUMO (73%), HOMO->L+2 (10%)	6.2874/295	0.0666
10	H-5->LUMO (82%)	6.4165/286	0.2481
11	H-6->LUMO (19%), H-1->L+2 (56%)	6.4904/284	0.0021
12	H-6->LUMO (73%), H-1->L+2 (12%)	6.7253/277	0.0000
13	H-1->L+3 (34%), HOMO->L+3 (61%)	6.7418/269	0.0227
14	H-2->L+1 (25%), H-1->L+4 (16%), HOMO->L+4 (43%)	6.9307/263	0.0194
15	H-2->L+1 (59%), H-1->L+4 (12%), HOMO->L+4 (18%)	6.9877/259	0.0000
16	H-7->LUMO (79%)	7.0157/245	0.0064

17	H-3->L+1 (66%)	7.0428/220	0.0033
18	H-1->L+3 (44%), HOMO->L+3 (30%)	7.0975/204	0.0027
19	H-4->L+1 (39%), HOMO->L+5 (16%)	7.1621/198	0.0000
20	H-4->L+1 (30%), H-2->L+2 (15%)	7.2400/195	0.7154

Reference

[1]B. O'Regan, M. Gratzel, Nature 353 (1991) 737-739.

[2]M. Gratzel, Nature 414 (2001) 338-344.

[3]N.G. Park, K. Kim, Phys. Status Solidi a. 205 (2008) 1895-1904.

[4]Y. Chiba, A. Islam, Y. Watanabe, R. Komiya, N. Koide, L. Han, Jpn. J. Appl. Phys 45 (2006) L638-L640.

[5]X.H. Zhang, C. Li, W.B. Wang, X.X. Cheng, X.S. Wang, B.W. Zhang, J. Mater.Chem. 17 (2007) 642-649.

[6]M. Liang, W. Xu, F. Cai, P. Chen, B. Peng, J. Chen, Z. Li, J. Phys. Chem. C, 111 (2007) 4465-4472.

[7]W. Xu, B. Peng, J. Chen, M. Liang, F. Cai, J. Phys. Chem. C, 112 (2008) 874-880.

[8]S. Ito, H. Miura, S. Uchida, M. Takata, K. Sumioka, P. Liska, P. Comte, P. Pechy, M. Gratzel, Chem. Commun. (2008) 5194-5196.

[9]M.J. Frisch, G.W. Trucks, H.B. Schlegel, G.E. Scuseria, M.A. Robb, J.R. Cheeseman, J.A. Montgomery Jr., T. Vreven, K.N. Kudin, J.C. Burant, J.M. Millam, S.S. Iyengar, J. Tomasi, V. Barone, B. Mennucci, M. Cossi, G. Scalmani, N. Rega, G.A. Petersson, H. Nakatsuji, M. Hada, M. Ehara, K. Toyota, R. Fukuda, J. Hasegawa, M. Ishida, T. Nakajima, Y. Honda, O. Kitao, H. Nakai, M. Klene, X. Li, J.E. Knox, H.P. Hratchian, J.B. Cross, C. Adamo, J. Jaramillo, R. Gomperts, R.E. Stratmann, O. Yazyev, A.J. Austin, R. Cammi, C. Pomelli, J.W. Ochterski, P.Y. Ayala, K. Morokuma, G.A. Voth, P. Salvador, J.J. Dannenberg, V.G. Zakrzewski, S.Dapprich, A.D. Daniels, M.C. Strain, O. Farkas, D.K. Malick, A.D. Rabuck, K. Raghavachari, J.B. Foresman, J.V. Ortiz, Q. Cui, A.G. Baboul, S. Clifford, J.Cioslowski, B.B. Stefanov, G. Liu, A. Liashenko, P. Piskorz, I. Komaromi, R.L. Martin, D.J. Fox, T. Keith, M.A. Al-Laham, C.Y. Peng, A. Nanayakkara, M. Challacombe, P.M.W. Gill, B. Johnson, W. Chen, M.W. Wong, C. Gonzalez, J.A. Pople, Gaussian 09, Gaussian, Inc., Pittsburgh, PA, 2009.

[10] B. Miehlich, A. Savin, H. Stoll, H. Preuss, Chem. Phys. Lett. 157 (1989) 200-206.

[11] C. Lee, W. Yang, R.G. Parr, Phys. Rev. B. 37 (1988) 785-789.

[12] V. Barone, M. Cossi, J. Phys. Chem. A, 102 (1998) 1995-2001.

[13] M. Cossi, N. Rega, G. Scalmani, V. Barone, J. Comput. Chem. 24 (2003) 669-681.

[14] M.K. Nazeeruddin, F. De Angelis, S. Fantacci, A. Selloni, G. Viscardi, P. Liska, S.Ito, B. Takeru, M. Gratzel, J. Am. Chem. Soc. 127 (2005) 16835-16847.

[15] M.J. Lundqvist, M. Nilsing, P. Persson, S. Lunell, Int. J. Quantum Chem. 106 (2006) 3214-3234.

[16] D.F. Waston, G.J. Meyer, Annu. Rev. Phys. Chem. 56 (2005) 119-156.

[17] C. R. Zhang, H. S. Chen, and G. H. Wang, Chem. Res. Chin. U. 20 (2004) 640-646.

[18] Y. Sun, X. Chen, L. Sun, X. Guo, W. Lu, Chem.Phys. Lett. 381 (2003) 397-403.

[19] O. Christiansen, J. Gauss, J. F. Stanton, Chem.Phys. Lett. 305 (1999) 147-155.

[20] Z. S. Wang, Y. Y. Huang, C. H. Huang, J. Zheng, H.M. Cheng, S. J. Tian, Synth. Met. 14 (2000) 201-207.

[21] C.R. Zhang, Y.Z. Wu, Y.H. Chen, H.S. Chen, Acta Phys. Chim. Sin. 25 (2009) 53-60.

[22] A. Seidl, A. Gorling, P. Vogl, J. A. Majewski, M. Levy, Phys. Rev. B 53 (1996) 3764-3774.

[23] K. Hara, T. Sato, R. Katoh, A. Furube, Y. Ohga, A. Shinpo, S. Suga, K. Sayama, H.Sugihara, H. Arakawa, J. Phys. Chem. B. 107 (2003) 597-606.

[24] C.R. Zhang, Z.J. Liu, Y.H. Chen, H.S. Chen, Y.Z. Wu, L.H. Yuan, J. Mol. Struct. (THEOCHEM) 899 (2009) 86-93.